

Homoclinic bifurcations in a liquid crystal flow

By T. PEACOCK[†] AND T. MULLIN

Department of Physics and Astronomy, Manchester University, Manchester, M13 9PL, UK

(Received 28 July 1999 and in revised form 27 September 2000)

The results of an experimental study of electrohydrodynamic convection in a liquid crystal are presented. Investigations concerned a small-aspect-ratio device so that finite geometry effects could be exploited to study the mechanisms by which complicated flows were organized. The results have been related to ideas on Shil'nikov dynamics and gluing bifurcations in low-dimensional dynamical systems.

1. Introduction

The work of Shil'nikov (1965) and Sparrow (1982) initiated the notion that homoclinic bifurcations are important in providing organizing centres for chaotic dynamics. Subsequently, experimental investigations of the transition to disordered fluid motion have sought to directly interpret observed behaviour in terms of these low-dimensional models. Studies have principally focused on the problems of Taylor–Couette flow between rotating cylinders and Rayleigh–Bénard convection in heated fluid layers. A modern review of this work is given by Cross & Hohenberg (1993) who also discuss applications in other fields. Numerical studies looking to identify homoclinic bifurcations in fluid systems have typically been concerned with models comprising sets of ordinary differential equations that arise as a projection of the governing equations of motion, with the classic example being that of Lorenz (1963). The behaviour found in these models is often difficult to reproduce experimentally. Nevertheless, they are instructive since they often highlight physically relevant and important ideas.

Using a combined numerical and experimental approach, a clear example of complicated dynamics in Taylor–Couette flow arising via a homoclinic bifurcation was reported by Mullin & Price (1989). In this instance a model was proposed for the behaviour, based on numerical results obtained using the Navier–Stokes equations by Mullin, Tavener & Cliffe (1989). In general, however, establishing a rigorous connection with physical flow problems has proven difficult, and it remains an outstanding problem to successfully relate the mathematics directly to experiments.

A flow problem that has become the focus of recent attention is convection in an electrically driven nematic liquid crystal, as reviewed by Kramer & Pesch in the book by Buka & Kramer (1996). A nematic is a complex fluid composed of rod-like molecules which possess orientational but not positional order. In practice it is possible to impose a preferred orientation on the director (a unit vector that characterizes local molecular orientation) by using minor forces, such as the guiding effect provided by surface treatment of bounding walls. A nematic exhibits complicated flow properties due to a coupling between translational and orientational motions of the

[†] Present address: Department of Mathematics, Massachusetts Institute of Technology, Cambridge, MA, USA.

molecules. If an electric field is applied to an appropriately aligned nematic confined between parallel glass plates, convection can occur above a critical field strength. This phenomenon is commonly known as electroconvection, and was first explained by Helfrich (1969). Associated with the convection is a distortion of the director field, which is manifested as a spatially varying refractive index. This enables flow to be observed directly as an intensity pattern formed by the focusing and defocusing of transmitted light.

Experimental investigations of electroconvection have typically been concerned with large-aspect-ratio systems, containing many convection rolls. Under these conditions it is assumed that one can describe the onset of convection, and subsequent transitions, using general arguments about pattern formation in non-equilibrium systems (Buka & Kramer 1996). In these circumstances it is difficult to investigate low-dimensional dynamics since the multiplicity of flows can be immeasurably large. Furthermore, the potential for clear observations is obscured by inevitable fluctuations that cause the system to jump between the many coexisting states. However, small-aspect-ratio electroconvection experiments can exhibit low- and high-dimensional behaviour (Tsuchiya, Horie & Itakura 1988; Peacock, Binks & Mullin 1999), providing an opportunity for detailed investigation of the transition to complicated fluid motion in a novel fluid system. In addition, an earlier investigation by Binks & Mullin (1997) has shown that the selection of the steady solution set can be understood in terms of ideas from singularity theory.

Here results are presented of an experimental investigation of flows in a small-aspect-ratio liquid-crystal cell. Within two distinct regions of parameter space this system behaved in a manner consistent with established models of homoclinic bifurcations. Before presenting these results, the experimental arrangement is described, along with some general observations on the flows involved.

2. The experiment

The liquid crystal cell comprised a $46 \pm 1.0 \mu\text{m}$ thick layer of nematic BDH-17886† sandwiched between two optically flat glass plates, and a schematic of this device is shown in figure 1. An indium-tin oxide line electrode was etched onto the inner surface of each plate. On the upper glass plate the width of the line electrode was $188.6 \pm 2.0 \mu\text{m}$ and on the bottom plate the width was $183.8 \pm 2.0 \mu\text{m}$. The arrangement of the plates was such that, when viewed from above, the line electrodes overlapped at right angles. This created an active region of aspect ratio $4.0 \pm 0.1 : 4.1 \pm 0.1 : 1.0$ to which an a.c. electric field could be applied. Using a sodium vapour lamp, Newton's fringes were observed and the maximum depth variation across the active region of the cell was calculated to be $0.02 \mu\text{m}$. Alignment of the material, which was parallel to the lower electrode, was obtained using a rubbed layer of poly-vinyl alcohol spin coated on top of the electrodes. The cell was mounted on a microscope translation stage and maintained at a constant temperature of $32.0 \pm 0.02^\circ\text{C}$. Applied a.c. voltages were of the order of $10V_{rms}$ and had a frequency of the order of 600 Hz. These parameters had a long-term stability of better than 0.5%. Light transmitted through the cell was imaged using a CCD camera and a computer imaging system. To facilitate flow visualization the plane of focus of the microscope was positioned above the liquid-crystal cell so that bright intensity lines corresponded to upwards fluid motion and fainter intensity lines to downwards fluid motion (Rehberg, Horner & Hartung 1991).

† Made by Merck Ltd, Merck House, Poole, Dorset, BH15 1TD, UK.

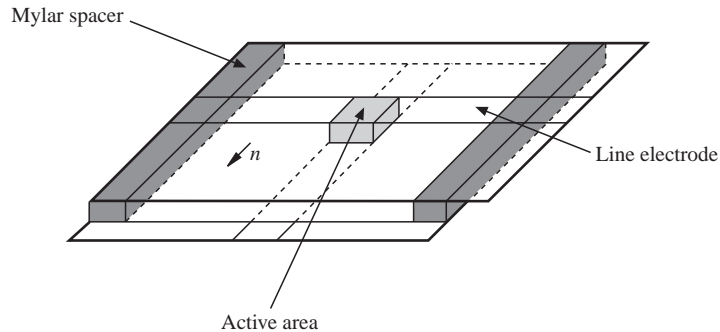


FIGURE 1. Schematic of the liquid-crystal cell. The unit vector n indicates the preferred molecular orientation, which is parallel to the lower line electrode.

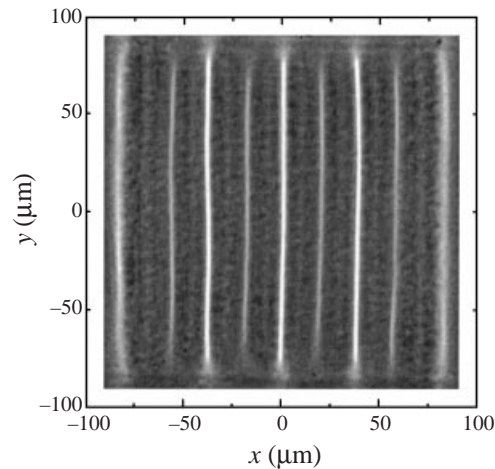


FIGURE 2. Image of eight-roll flow. A set of x, y reference axes have been placed around the image to provide a coordinate system for locating flow features. The units for the axes are microns and the original alignment of the director is left to right.

As described by Binks & Mullin (1997), within a particular voltage and frequency range an eight-roll flow was primary according to the definition of Benjamin (1978), i.e. it smoothly evolved from the undisturbed nematic as the voltage, V , was continuously increased or the frequency, F , was continuously reduced. An image of the eight-roll flow is presented in figure 2, in which bright lines correspond to upwards flow and fainter lines to downwards flow. A set of reference axes have been included in the figure to aid the description of flow features later on in the paper. In neighbouring regions of parameter space the primary flow comprised six or ten convection rolls. By systematically varying V and F experimental bifurcation sequences could be determined for the eight-roll flow. For the purpose of recording transition values a non-dimensional scheme similar to that introduced by Kai & Hirakawa (1978) was used, where a voltage reference value, V_{ref} , was defined to be the lowest voltage at which the eight-roll flow was primary. In a like manner, the frequency reference value, F_{ref} , was defined to be the highest frequency at which a six-roll flow was primary. The non-dimensionalized variables were therefore $V = V/V_{ref}$ and $F = F/F_{ref}$. The location of a bifurcation point in (V, F) parameter space could typically be determined with an accuracy of 0.1%.

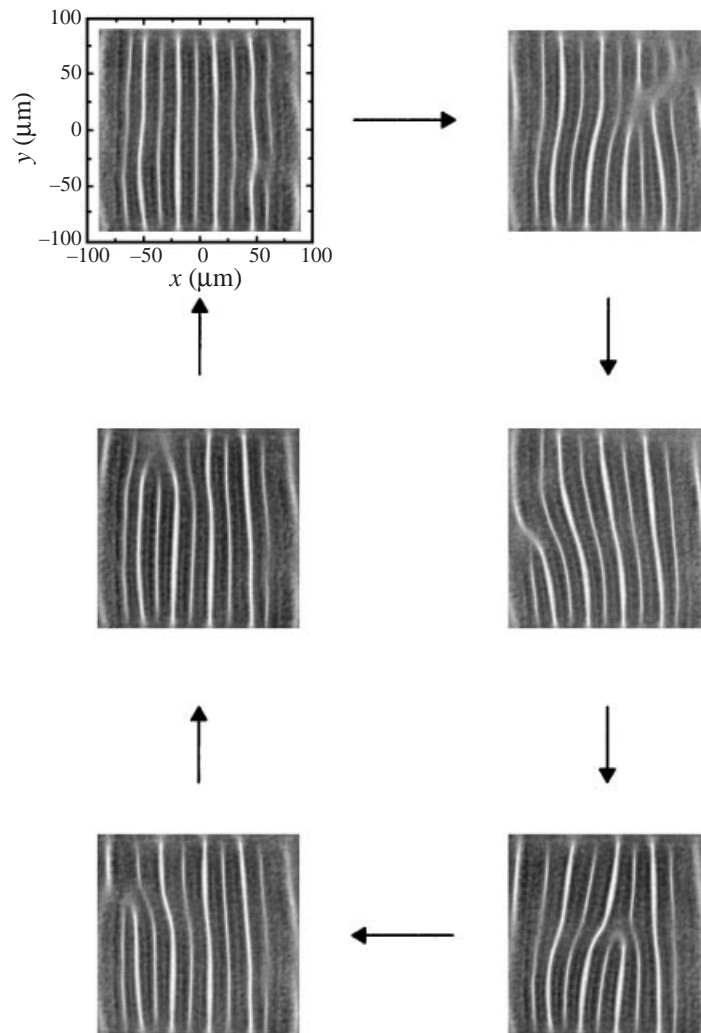


FIGURE 3. Sequence of images taken from the mixed-mode flow at $(V, F) = (1.588, 1.409)$. This flow comprises a combination of eight and ten convection rolls.

3. Experimental observation of Shil'nikov dynamics

For $V > 1.037$ the eight-roll flow underwent a Hopf bifurcation as F was continuously reduced, as reported in Peacock *et al.* (1999). The resulting periodic flow comprised a 'breaking' and 'joining' of the convection rolls. As F was further reduced the eight-roll time-dependent flow underwent a hysteretic transition to a time-dependent mixed-mode state. A sequence of images depicting the mixed-mode state is presented in figure 3. In the top-left image the system resembles a steady ten-roll flow, which then evolves into an oscillating pattern comprising features of both eight and ten convection rolls, and contains a so-called 'defect' (Braun, Rasenat & Steinberg 1991; Kaiser & Pesch 1993) where the rolls do not match across the middle of the cell. The amplitude of oscillation decreases and the flow then returns to ten convection rolls before the cycle repeats.

Further illustration of the mixed-mode dynamics is provided by the time series

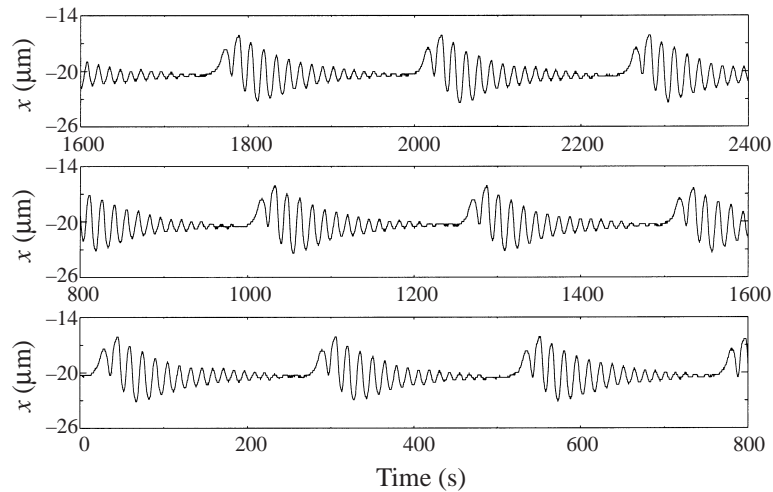


FIGURE 4. Time series taken from the mixed-mode at $(V, F) = (1.588, 1.409)$. The ordinate x is the lateral position of the selected maximum in the intensity pattern.

in figure 4. This was obtained in the following manner. Across a horizontal row of pixels there existed clear intensity maxima that corresponded to upwards flow. For eight-roll flow there were three such maxima and for ten-roll flow there were four. One maximum was selected and its horizontal displacement tracked throughout the oscillation. This measure was first used by Yang *et al.* (1986) and the nature of the time series obtained was, for the most part, found to be independent of the choice of intensity maximum. For the purpose of obtaining the time series presented in this section the chosen maximum was at the location $(x, y) = (-20, -50)$ as this gave the best signal-to-noise ratio. In figure 4 a flat line in the time series corresponds to the system resembling a steady ten-roll flow. Mixed-mode oscillations, containing features of both eight and ten convection rolls, evolve rapidly from this state and then decay as the system returns to the steady ten-roll flow. This sequence of events is then repeated in a highly regular manner. For the time series presented the duration of a mixed-mode oscillation was of the order of 250 s.

The subsequent evolution of the mixed-mode flow with variation of the control parameters was analogous to a low-dimensional model described by Shil'nikov (1965). A description of this model is given in the following subsection. The experimental results are then presented and a comparison is drawn with the model.

3.1. The Shil'nikov mechanism

A phase portrait of an orbit homoclinic to a saddle-focus is shown in figure 5, depicting trajectories that spiral in on a plane towards the unstable fixed point and are ejected in a perpendicular direction. Shil'nikov (1965) first proved theorems concerning the stability and existence of periodic orbits in the neighbourhood of phase space containing such an orbit. Thereafter, an explicit description of how a periodic orbit becomes homoclinic to a saddle-focus as a bifurcation parameter is varied was provided by Glendinning & Sparrow (1984).

Assuming the eigenvalues of the saddle-focus to be of the form λ_1 and $-\lambda_2 \pm i\omega$ ($\lambda_1, \lambda_2, \omega > 0$) the nature of the approach to homoclinicity is determined by the ratio of the stable and unstable eigenvalues $\delta = \lambda_2/\lambda_1$. When $\delta > 1$ the orbit period

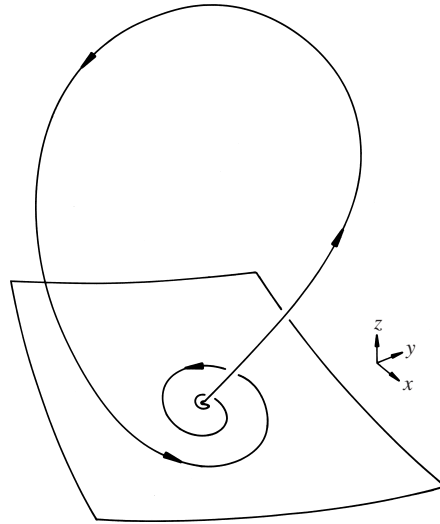
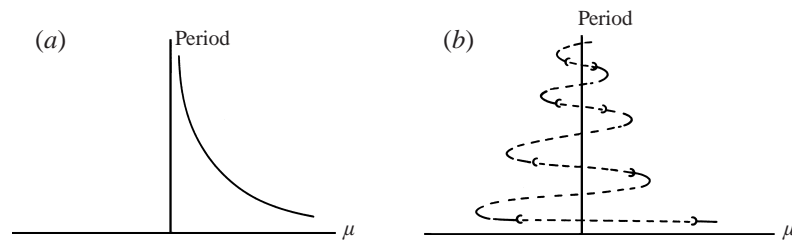


FIGURE 5. Phase portrait of an orbit homoclinic to a saddle-focus.

FIGURE 6. Bifurcation diagrams illustrating the homoclinic approach to a saddle focus. Solid (dashed) lines indicate stable (unstable) periodic orbits. (a) $\delta > 1$, (b) $1/2 < \delta < 1$.

increases monotonically towards infinity as the bifurcation point is reached, and the periodic orbit is stable throughout the homoclinic approach. An illustration of this behaviour is given in figure 6(a), which contains a bifurcation diagram of the period plotted as a function of the bifurcation parameter μ . When $1/2 < \delta < 1$ the scenario is more complex and a homoclinic orbit arises in a sequence of periodic folds and period-doubling cascades, as shown by the schematic bifurcation diagram in figure 6(b). For parameter values on either side of the bifurcation point a finite number of stable periodic orbits coexist. The period-doubling cascades can give rise to attracting chaotic solutions as discussed by Gaspard, Kapral & Nicolis (1984). The continuous nature of the transition between the two bifurcation diagrams shown in figure 6 as δ passes through 1 was suggested by Glendinning & Sparrow (1984), and has been confirmed experimentally and numerically by Healey *et al.* (1991) in a nonlinear oscillator. Finally, when $\delta < 1/2$ there remains a similar bifurcation structure to that shown in figure 6(b). However, the periodic orbits generated are unstable and therefore not directly observable in an experiment.

3.2. Experimental results

Upon individually varying either V or F no appreciable change in the period of the mixed-mode flow was found before the system collapsed onto a singly periodic eight-roll mode. Since it is reasonable to expect a non-trivial relationship between

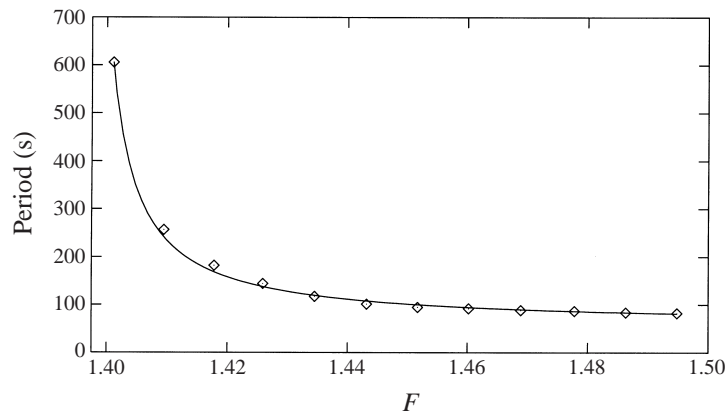


FIGURE 7. The period dependence of the mixed mode. Here F has been used as the abscissa. Since measurements were taken along a linear path in (V, F) parameter space a qualitatively similar graph could be obtained using V as the abscissa. A logarithmic form could not be fitted to the results and the solid line drawn through the data points serves only to guide the eye.

experimental control parameters and those of an ordinary differential equation model, we used alternative paths in the experimental control parameter plane that entailed a simultaneous variation of both parameters, in search of a definite change in period. By doing so, a monotonic increase in the period of the mixed mode was revealed. A systematic study of the period of oscillation along a straight path in parameter space between $(V, F) = (1.745, 1.512)$ and $(1.575, 1.401)$ was undertaken, and the results are presented in figure 7. The period was measured using the autocorrelation function of time series such as that shown in figure 4. Over the range investigated the period rose from 82 to 606 s, at which point the system collapsed back onto a singly periodic eight-roll flow. The gain in period was manifested as an increasing persistence of the high-frequency oscillations.

The sequence of events described for the mixed-mode flow is analogous to the homoclinic approach of a periodic orbit to a saddle-focus when $\delta > 1$. In the abstract model the period of the orbit tends to infinity by winding itself around the unstable fixed point, and such behaviour was manifested as increasingly persistent high-frequency oscillations. However, neither of the control parameters could be individually related to the model parameter μ . Rather, the linear path traversed in (V, F) parameter space corresponded to a seemingly monotonic variation of μ . As suggested by Gaspard (1990), an attempt was made to fit a logarithmic curve of the form

$$t = t_0 + \alpha \ln(F - F_c)$$

to the results, where t is the period of oscillation, t_0 and α are fitting parameters, F is the non-dimensional frequency and $F_c = 1.4$ was the critical frequency at which the system collapsed onto another state. The curve fitting routine used a gradient expansion algorithm to compute a nonlinear least-squares fit to the logarithmic function. However, it was not possible to obtain a fit to the analytical form, indicating a nonlinear relation between abstract and experimental parameters over the region of parameter space investigated.

Further support for this interpretation is provided by the phase portrait presented in figure 8, which was reconstructed from a time series taken at $(V, F) = (1.642, 1.443)$ using the now standard technique of method of delays augmented with singular value decomposition suggested by Broomhead & King (1986). This technique calculates an

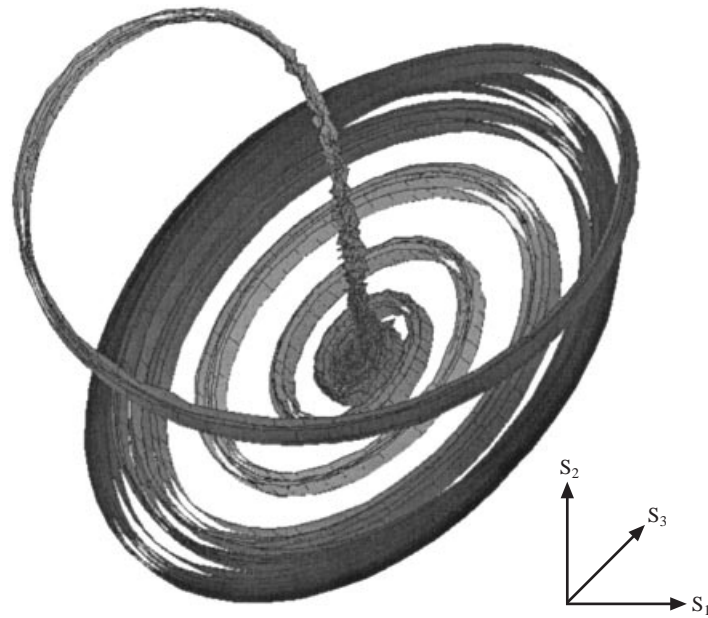


FIGURE 8. Phase portrait representation of the mixed-mode dynamics, reconstructed from a time series taken at $(V, F) = (1.642, 1.443)$. S_1 , S_2 and S_3 are projection axes for the first three singular vectors.

optimal basis for the projection of the attractor which has been reconstructed from the time series, and the reader is referred to Mullin (1993) for further details. The reconstructed attractor in figure 8 has been plotted on a coordinate system of the first three singular vectors and it shows that the motion can be represented as taking place near a saddle-focus in the reconstructed phase space. At its centre the attractor contains an unstable fixed point corresponding to ten-roll flow. The initial part of the mixed-mode oscillation, in which there is a transition from a ten-roll flow to a mixed eight/ten-roll state, is represented by a trajectory departing vertically from the centre. The subsequent return to a steady ten-roll flow is then portrayed by orbits spiralling in towards the unstable fixed point. Shading in the phase portrait indicates the rate of change along a trajectory, with dark being fast and light being slow. The high concentration of points near the centre of the attractor indicates that the trajectories spend a relatively long time in the region of the unstable fixed point, consistent with δ being greater than 1.

On traversing a linear path in parameter space parallel to that previously followed, between $(V, F) = (1.745, 1.495)$ and $(1.575, 1.384)$, the evolution of the mixed-mode flow was found to change significantly. Rather than displaying a monotonic increase in period, the dynamics first became disordered. The seemingly chaotic behaviour is illustrated by the time series presented in figure 9. In contrast to the time series presented in figure 4, it can be seen that the high-frequency oscillations persisted for irregular intervals. As the parameters were further reduced the system then collapsed back onto the singly periodic mode presented in figure 10(a). This flow was again a mixed eight/ten-roll state, and was not a transient but persisted over an extended region of parameter space. Upon repeating the traverse of parameter space a number of times the mixed-mode flow was observed to collapse onto several different periodic flows comprising both eight and ten convection rolls. Image sequences of two other

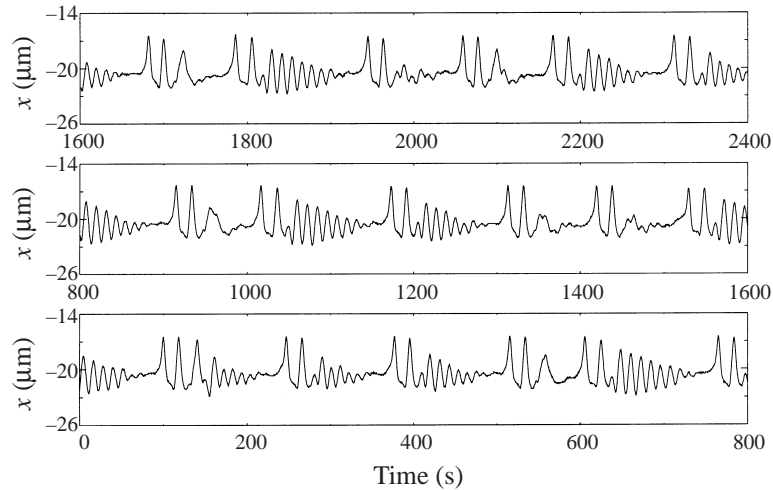


FIGURE 9. Seemingly chaotic time series taken from the mixed-mode at $(V, F) = (1.655, 1.435)$.

such flows are shown in figures 10(b) and 10(c), both of which coexisted with that shown in figure 10(a). These flows are also seen to contain ‘defects’ where there is a discontinuity in the number of convection rolls.

The sequence of events along the alternative path in parameter space is consistent with the model problem of Glendinning & Sparrow when $1/2 < \delta < 1$. As illustrated in figure 6, under these circumstances a finite number of stable periodic orbits can coexist on either side of the homoclinic bifurcation point. Such solutions were manifested as the coexisting periodic flows presented in figure 10. Furthermore, within this range of δ chaotic solutions are known to arise through period-doubling bifurcations. In the experiment it was not possible to identify a definite period-doubling sequence as the mechanism by which this behaviour arose. In principle such behaviour must have existed, but presumably over such a small parameter range that it could not be resolved. However, the observation of irregular mixed-mode behaviour is consistent with the existence of such chaotic solutions.

The experimental results presented here provide a strong body of evidence for the existence of Shil’nikov dynamics in the liquid-crystal cell. An important point of note, however, is that in the Shil’nikov model the transition between bifurcation sequences from $\delta > 1$ to $\delta < 1$ is a smooth one. This has been observed both experimentally and numerically by Healey *et al.* (1991) in a Van der Pol oscillator, whose behaviour is governed by ordinary differential equations. For the liquid-crystal cell, a system governed by partial differential equations, there was no obvious relation between the two experimental parameters V and F and the parameters μ and δ in the model. Thus it was unclear how a linear path in (V, F) parameter space traversed the two-dimensional (μ, δ) bifurcation set of the abstract system. This being the case, it was impractical to conduct more detailed investigations of the transition between the two qualitatively different regimes described, but the evidence of the qualitative change in the solution structure is consistent with a change from $\delta > 1$ to $\delta < 1$.

4. Experimental observation of a gluing bifurcation

In a parameter regime surrounding $V = 0.990$ and $F = 0.750$ there existed behaviour consistent with another form of homoclinic bifurcation, which is distinctly

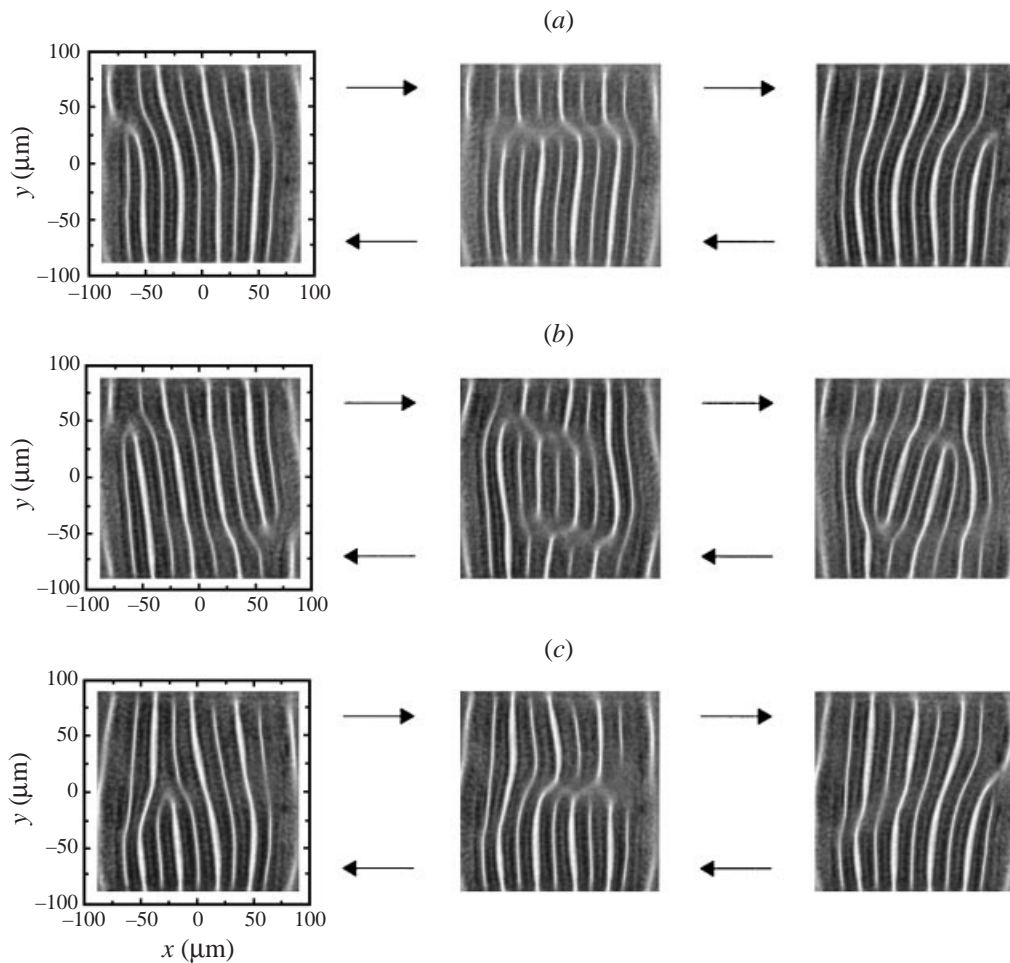


FIGURE 10. Singly periodic flows arising from the collapse of the mixed mode. In each case, viewing the images from left to right and then back again corresponds to one oscillation. The flows presented in (a), (b) and (c) coexisted with each other.

different from that previously described. Here, using F as the bifurcation parameter, investigations focused on a pair of symmetry-broken time-dependent eight-roll flows, shown in figure 11. The time-dependent states have been labelled 0 and 1, and were characterized by a periodic ‘tilting’ of the convection rolls in one half of the flow domain, with a typical period of 36 s. These flows existed as secondary modes that could be obtained by virtue of a discontinuous change in the control parameters, and were related to each other through a mid-plane reflection symmetry. At low enough values of F the 0 and 1 modes could no longer be realized, and were replaced by a large-amplitude periodic solution, called the 01 mode, which typically had a period of 70 s. A sequence of images taken from the 01 mode, which comprised alternate tilting in each half of the flow domain, is presented in figure 12.

The sequence of events described is suggestive of a ‘gluing bifurcation’. A description of gluing bifurcations is given in the next subsection, followed by a presentation of more detailed experimental results.

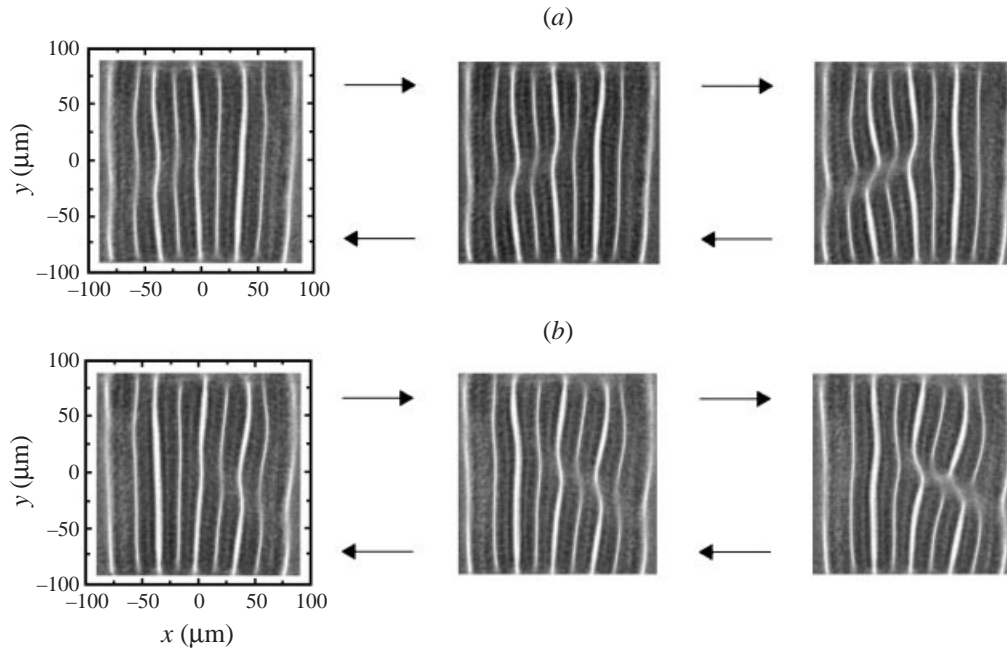


FIGURE 11. Sequences of images taken from the singly periodic 0 and 1 modes. (a) The singly periodic mode 0. (b) The singly periodic mode 1. Viewing the images from left to right and then back again corresponds to one oscillation.

4.1. Gluing bifurcations

The term ‘gluing bifurcation’ refers to a homoclinic bifurcation in which a pair of periodic orbits come together at a saddle point and form a large periodic orbit that is essentially a combination of the separate orbits, and was introduced by Couillet, Gambaudo & Tresser (1984). As such, the two initial orbits can be thought of as having been glued together at the saddle point as a parameter is changed. This behaviour typically occurs in systems of ordinary differential equations possessing a reflection symmetry that maps a saddle point onto itself. In such systems the existence of an orbit homoclinic to the saddle point requires the existence of another, which is the image of the first under the reflection.

In a three-dimensional system with a reflection symmetry, a gluing bifurcation can occur in one of three configurations. Two of these, the ‘figure of eight’ and ‘butterfly’ configurations, are presented in figures 13(a) and 13(b) respectively. The third configuration involves a pair of orbits homoclinic to a saddle-focus (Gambaudo, Glendinning & Tresser 1984) and is not considered here. Assuming the saddle point to have an unstable eigenvalue λ_1 and a pair of stable eigenvalues $-\lambda_3 < -\lambda_2 < 0$, then the value of $\delta = \lambda_2/\lambda_1$ is significant. If $\delta > 1$ a gluing bifurcation occurs for both configurations (Couillet *et al.* 1984; Gambaudo, Glendinning & Tresser 1985) and the orbits involved are stable. For $\delta < 1$ a gluing bifurcation occurs for the figure-of-eight configuration, but the orbits involved are unstable and cannot be realized in an experiment (Glendinning 1989). No gluing bifurcation occurs for the butterfly configuration with $\delta < 1$. Instead a pair of unstable homoclinic orbits arise through a homoclinic explosion and no large-amplitude periodic solution exists beyond the bifurcation point (Sparrow 1982).

In the absence of perfect reflection symmetry a gluing bifurcation has a codimension

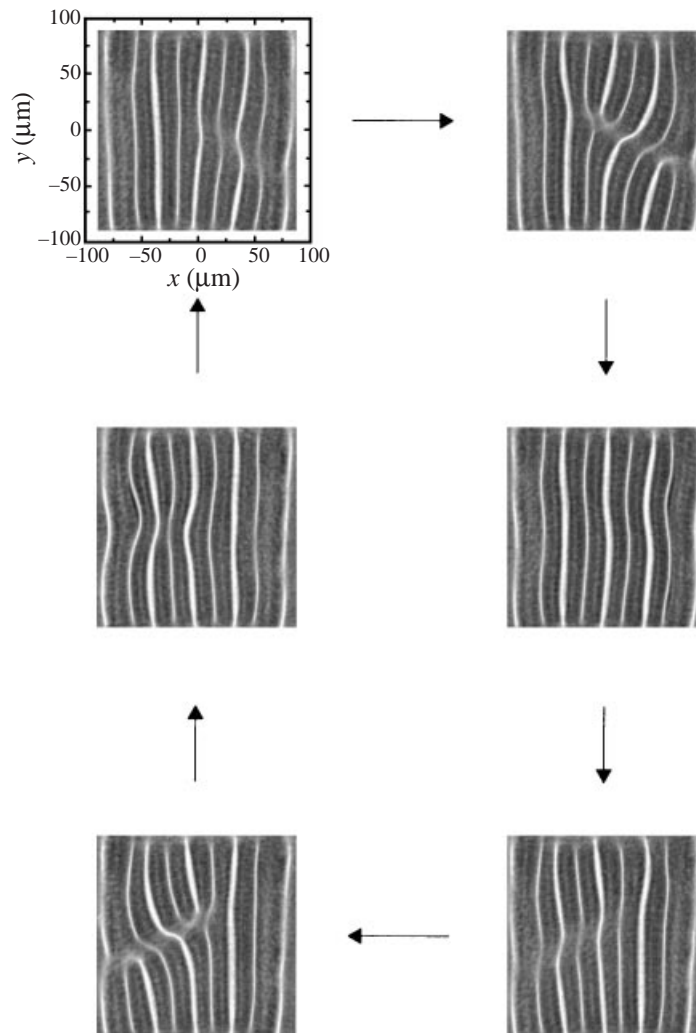


FIGURE 12. A sequence of images taken from the singly periodic mode 01.

of two, since one parameter is required to control the homoclinic connection of each periodic orbit. A bifurcation set for the imperfect figure-of-eight and butterfly configurations with $\delta > 1$ is shown in figure 14(a). It comprises a two-dimensional parameter plot, in which it is assumed that independent control of the homoclinic connections is provided by the parameters μ_0 and μ_1 . Along $\mu_0 = \mu_1$ the system is symmetric. As this path is traversed a gluing bifurcation occurs at the origin, in which the stable orbits 0 and 1 combine to form the stable 01 orbit, which exists in the unshaded region of figure 14(a) where $\mu_1, \mu_2 > 0$. If an asymmetric parameter path is followed a more complicated bifurcation sequence occurs. For $\mu_0, \mu_1 < 0$ the homoclinic approaches of the 0 and 1 orbits take place as μ_0 or μ_1 respectively tend to zero. Upon crossing an axis one of the orbits is destroyed in a homoclinic bifurcation, while the other persists. Within the shaded regions there exists an intricate sequence of homoclinic bifurcations that create and destroy complicated periodic orbits (Turaev & Shil'nikov 1987; Gambaudo, Glendinning & Tresser 1987). The nature of this

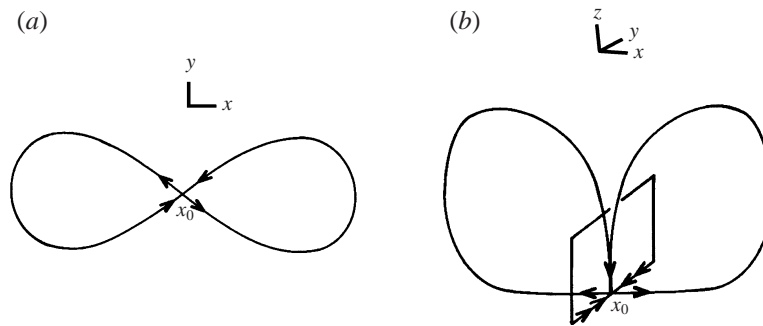


FIGURE 13. Gluing bifurcations at a saddle point x_0 . (a) Figure of eight. (b) Butterfly.

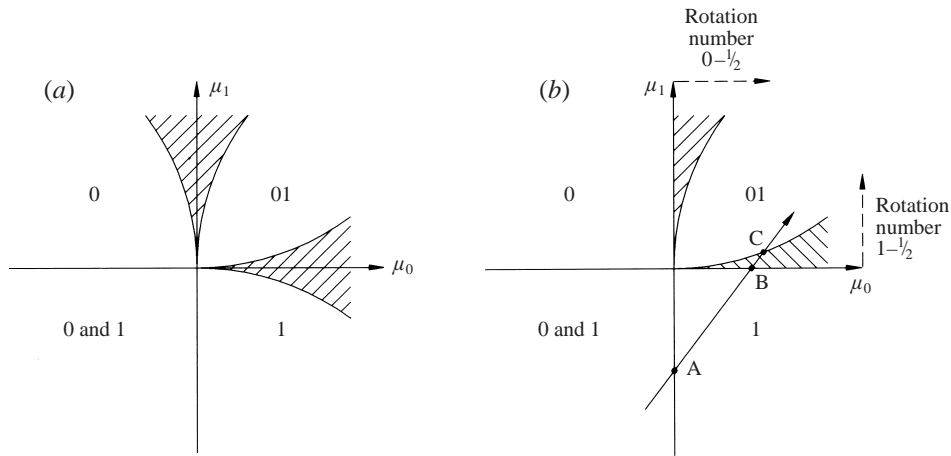


FIGURE 14. (a) Bifurcation set for imperfect figure-of-eight and butterfly gluing bifurcations with $\delta > 1$. (b) Detailed bifurcation set for the imperfect butterfly gluing bifurcation with $\delta > 1$.

sequence is dependent on the configuration, figure of eight or butterfly, and the orientability (twist) of the orbits (see Gambaudo *et al.* 1987; Wiggins 1988).

A more detailed diagram for the butterfly configuration with orientable orbits is presented in figure 14(b). In this case the shaded regions $\mu_0 < 0, \mu_1 > 0$ and $\mu_0 > 0, \mu_1 < 0$ in figure 14(a) contain trivial dynamics as discussed by Glendinning (1988). However, when μ_0 and μ_1 are both positive, at any parameter value within the shaded regions there is at most one stable periodic orbit. The trajectory of this orbit may be represented by a rotation number that can vary continuously and monotonically with one parameter when the other is held fixed. For example, if an asymmetric parameter path is traversed such as that shown through the points A, B and C in figure 14(b), an 011 orbit with rotation number $2/3$ can exist within the shaded region, corresponding to a trajectory that performs two 1 orbits for each 0 orbit. The rotation number of an orbit can become irrational, corresponding to an aperiodic, but not chaotic, solution.

Behaviour associated with gluing bifurcations has been reported in numerical models of fluid systems by Rucklidge (1992) and has been observed experimentally in optothermal nonlinear devices by Herrero *et al.* (1998). To the best of our knowledge there has been no clear observation of such behaviour in an experimental fluid system.

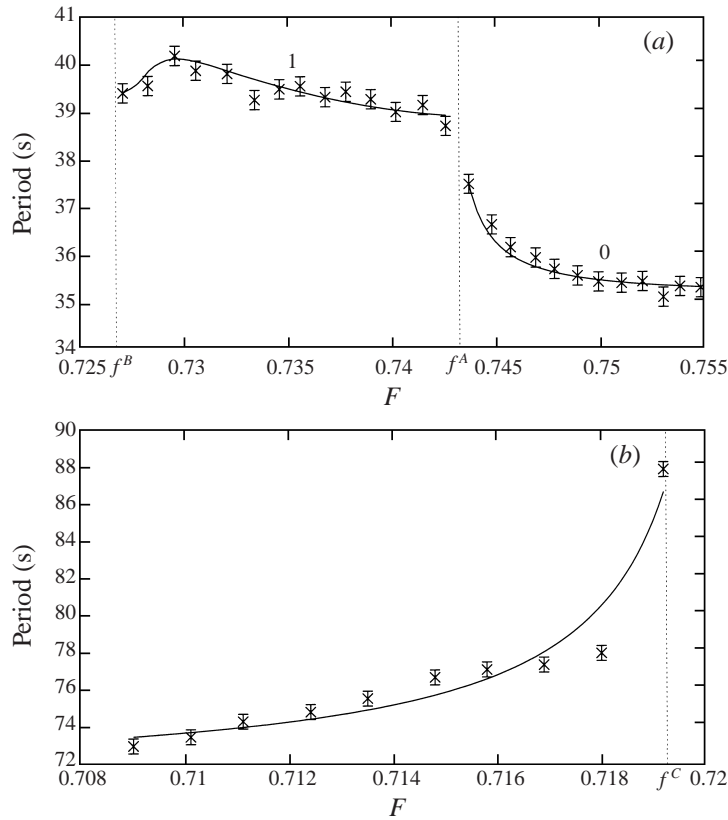


FIGURE 15. (a) Period dependence of the 0 and 1 modes. (b) Period dependence of the 01 mode. The fitted curves for the 0 and 01 modes are logarithmic and were obtained using a nonlinear least-squares fitting routine. The solid line drawn through the data points for the 1 mode serves only to guide the eye.

4.2. Experimental results

The value of V was fixed at 0.990 and F was used as the bifurcation parameter. The 0 mode was realized first, as this could be readily found. As F was reduced the period increased monotonically from 35.3 s towards 37.5 s at $F^A = 0.743$, and this behaviour is plotted in figure 15(a). Below F^A the 0 mode could no longer be maintained and the system jumped catastrophically onto the 1 mode, which had a period of 38.7 s. As F was further reduced the period of the 1 mode was found to increase to 40.2 s and then decrease to 39.4 s at $F^B = 0.727$, as shown in figure 15(a). Below F^B the 1 mode could no longer be maintained and the pattern comprised a seemingly random number of 1 oscillations for each 0 oscillation. The transition to irregular behaviour was reversible, so that the 1 mode could be regained by smoothly increasing F above F^B .

Upon reducing F below the critical value $F^C = 0.719$ the 01 mode was realized, in which convection rolls tilted alternately in each half of the flow domain. The transition to the 01 mode from the irregular regime was reversible, so that irregular behaviour could be regained by increasing F through F^C . In addition, the period of the 01 mode was found to increase monotonically from 73.0 to 87.3 s as F was increased towards the critical value F^C , as shown in figure 15(b).

The sequence of events described is analogous to an imperfect gluing bifurcation

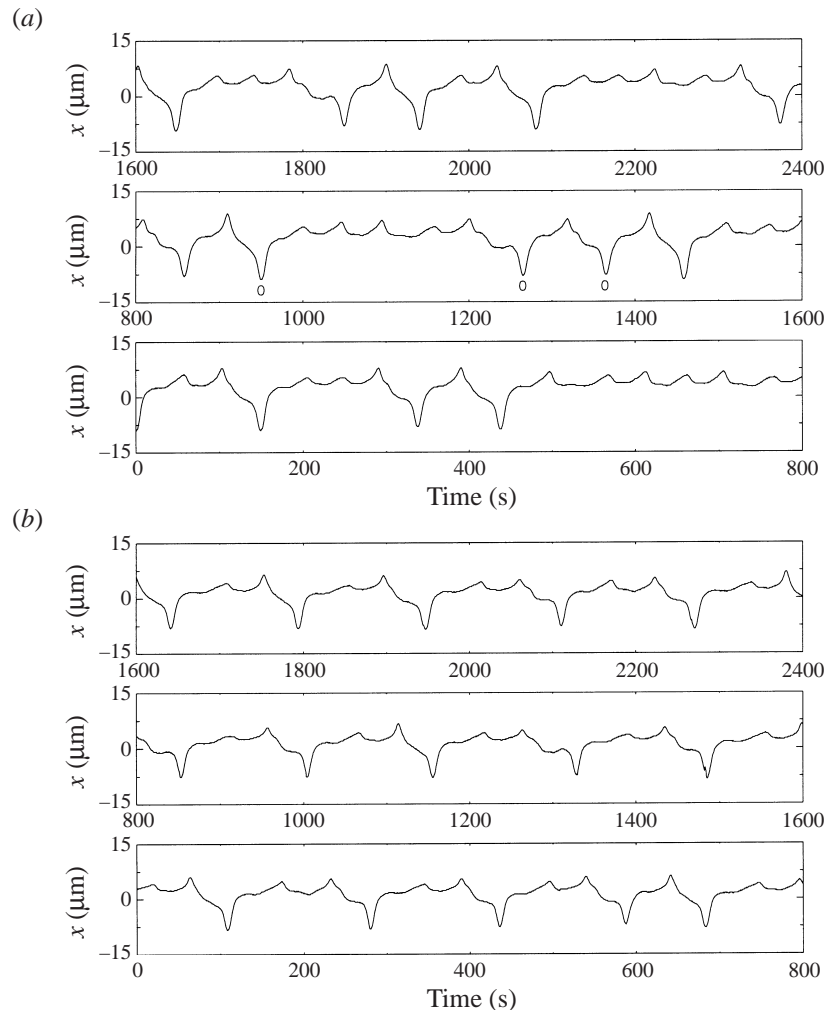


FIGURE 16. (a) Time series of irregular behaviour taken at $F = 0.725$. (b) Time series taken from the 011 mode at $F = 0.723$. The peaks and troughs respectively correspond to 1 and 0 oscillations.

in the butterfly configuration. Within the context of this model the 0 and 1 modes correspond to periodic orbits that combine to form a large-amplitude orbit, manifested as the 01 mode. Decreasing F was equivalent to traversing the asymmetric parameter path drawn in figure 14(b), and the parameter values F^A , F^B and F^C correspond to the points of homoclinic bifurcation labelled A, B and C respectively. Using the nonlinear least-squares curve fitting routine described earlier in the paper, the increase in period of the 0 and 01 modes preceding their disappearance was found to be logarithmic, consistent with these flows undergoing a homoclinic bifurcation (Gaspard 1990). However, the same behaviour could not be clearly identified for the 1 mode.

By analogy with the model of a gluing bifurcation, disconnection of the bifurcation sequence suggested a complicated solution structure may exist in the parameter range $F^B < F < F^C$. A detailed study of this parameter range was undertaken. To illustrate the nature of the dynamics in this regime, a time series taken at $F = 0.725$ is presented in figure 16(a). The time series was obtained using the technique described

in the previous section, and the location of the selected intensity maximum was $(x, y) = (0, -25)$. In the time series ‘troughs’ and ‘peaks’ respectively correspond to 0 and 1 oscillations, and examples have been labelled in figure 16. It can be seen that the flow performed a seemingly random number of 1 oscillations for each 0 oscillation. As F was decreased from F^B to F^C the average number of 1 oscillations for each 0 oscillation was observed to decrease. Furthermore, at $F = 0.723$ an 011 mode was revealed, in which the flow typically performed two 1 oscillations for each 0 oscillation. A time series taken from this flow is presented in figure 16(b). It was not possible to realize a flow that performed more than one 0 oscillation for each 1 oscillation.

The behaviour in the parameter regime between F^B and F^C further supports the analogy with a gluing bifurcation in the butterfly configuration. Observations of irregular flows correspond to having realized solutions with irrational rotation numbers. In principle a rotation number can be associated with each of the flows realized. However, the presence of thermal noise, which is known to have pronounced effects on electroconvection (Rehberg *et al.* 1991), was sufficient to mask the details of the motion so that it proved to be very difficult to obtain reliable quantitative estimates of the dynamics. The decrease in the average number of 1 oscillations for each 0 oscillation corresponds to the rotation number decreasing from 1 to $1/2$ as the path between points B and C is traversed in figure 14(b). Finally, the existence of the 011 mode corresponds to the realization of a solution with rotation number of $2/3$.

Results presented in this section strongly support the existence of a gluing bifurcation in the liquid-crystal cell. The presence of thermal noise in the system prevented a more quantitative investigation of the solution structure. Nevertheless, the qualitative and quantitative measurements presented here provide good agreement with theory.

5. Conclusions

We have demonstrated that homoclinic bifurcations can model some aspects of the transition to disordered motion in a complex fluid. Previous studies have typically concerned large-aspect-ratio systems containing many convection rolls. For these systems recent progress has been made using techniques for analysing pattern-forming instabilities and the consideration of ‘defect dynamics’ (Plaut *et al.* 1997; Pesch & Behn 1998), and it is interesting to note that some features of defect structure persist in our small-aspect-ratio system. In our view, progress with the equations of motion in the small-aspect-ratio case will require numerical simulation and although this remains a significant challenge to computation Tavener, Mullin & Blake (2001) have made advances. Nevertheless, by using careful experimental procedure we have uncovered complicated dynamical motion in a small-aspect-ratio system that can be directly related to relatively simple low-dimensional models.

This research was funded by the EPSRC and SHARP Labs Europe. T.P. was supported by The Packard Foundation during the writing up of this work.

REFERENCES

- BENJAMIN, T. B. 1978 Bifurcation phenomena in steady flows of a viscous fluid. Parts I & II. *Proc. R. Soc. Lond. A* **359**, 1–43.
- BINKS, D. J. & MULLIN, T. 1997 Cell number selection in electrohydrodynamic convection in liquid crystals. *Proc. R. Soc. Lond. A* **453**, 2109–2122.
- BRAUN, E., RASENAT, S. & STEINBERG, V. 1991 Mechanism of transition to a weak turbulence in extended anisotropic systems. *Europhys. Lett.* **15**, 597–602.

- BROOMHEAD, D. S. & KING, G. P. 1986 Extracting qualitative dynamics from experimental data. *Physica D* **20**, 217–236.
- BUKA, A. & KRAMER, L. 1996 *Pattern Formation in Liquid Crystals*. Springer.
- COULLET, P., GAMBAUDO, J. M. & TRESSER, C. 1984 Une nouvelle bifurcation de codimension-2: le collage de cycles. *C. R. Acad. Sci. Paris* **299**, 253–256.
- CROSS, M. C. & HOHENBERG, P. C. 1993 Pattern formation outside of equilibrium. *Rev. Mod. Phys.* **65**, 851–899.
- GAMBAUDO, J. M., GLENDINNING, P. A. & TRESSER, C. 1984 Collage de cycles et suites de Farey. *C. R. Acad. Sci. Paris* **299**, 711–714.
- GAMBAUDO, J. M., GLENDINNING, P. A. & TRESSER, C. 1985 Stable cycles with complicated structure. *J. Phys. Lett.* **46**, L653–L657.
- GAMBAUDO, J. M., GLENDINNING, P. A. & TRESSER, C. 1987 Stable cycles with complicated structure. In *Instabilities and Nonequilibrium Structures* (ed. E. Tirapegui & D. Villarroel), pp. 41–61. Reidel.
- GASPARD, P. 1990 Measurement of the instability rate of a far-from-equilibrium steady state at an infinite period bifurcation. *J. Phys. Chem.* **94** 1–3.
- GASPARD, P., KAPRAL, R. & NICOLIS, G. 1984 Bifurcation phenomena near homoclinic systems: a two parameter analysis. *J. Statist. Phys.* **35**, 697–727.
- GLENDINNING, P. A. 1988 Global bifurcations in flows. In *New Directions in Dynamical Systems* (ed. T. Bedford & J. Swift), pp. 120–149. Cambridge University Press.
- GLENDINNING, P. A. 1989 Global structure of homoclinic bifurcations: a combinatorial approach. *Phys. Lett. A* **141**, 391–396.
- GLENDINNING, P. & SPARROW, C. 1984 Local and global behaviour near homoclinic orbits. *J. Statist. Phys.* **35**, 645–696.
- HEALEY, J. J., BROOMHEAD, D. S., CLIFFE, K. A., JONES, K. A. & MULLIN, T. 1991 The origins of chaos in a modified Van der Pol oscillator. *Physica D* **48**, 322–339.
- HELFRICH, W. 1969 Conduction induced alignment of nematic liquid crystals: basic model and stability considerations. *J. Chem. Phys.* **51**, 4092–4105.
- HERRERO, R., FARJAS, J., PONS, R., PI, F. & ORRIOLS, G. 1998 Gluing bifurcations in optothermal nonlinear devices. *Phys. Rev. E* **57**, 5366–5377.
- KAI, S. & HIRAKAWA, K. 1978 Successive transitions in electrohydrodynamic instabilities of nematics. *Prog. Theor. Phys. Suppl.* **64**, 212–243.
- KAISER, S. N. & PESCH, W. 1993 Amplitude equations for the electrohydrodynamic instability in nematic liquid crystals. *Phys. Rev. E* **48**, 4510–4528.
- LORENZ, E. N. 1963 Deterministic nonperiodic flows. *J. Atmos. Sci.* **20**, 130–141.
- MULLIN, T. 1993 *The Nature of Chaos*. Oxford University Press.
- MULLIN, T. & PRICE, T. J. 1989 An experimental observation of chaos arising from the interaction of steady and time-dependent flows. *Nature* **340**, 294–296.
- MULLIN, T., TAVENER, S. & CLIFFE, K. A. 1989 An experimental and numerical study of a codimension-2 bifurcation in a rotating annulus. *Europhys. Lett.* **8**, 251–256.
- PEACOCK, T., BINKS, D. J. & MULLIN, T. 1999 From low- to high-dimensional dynamics in a microscopic fluid flow. *Phys. Rev. Lett.* **82**, 1446–1449.
- PESCH, W. & BEHN, U. 1998 Electrohydrodynamic convection in nematics. In *Evolution of Spontaneous Structures in Dissipative Continuous Systems* (ed. F. Busse & S. Mueller), pp. 335–383. Springer.
- PLAUT, E., DECKER, W., ROSSBERG, A. G. *et al.* 1997 New symmetry breaking in nonlinear electroconvection of nematic liquid crystals. *Phys. Rev. Lett.* **79**, 2367–2370.
- REHBERG, I., HORNER, F. & HARTUNG, G. 1991 The measurement of subcritical electroconvection. *J. Statist. Phys.* **64**, 1017–1023.
- REHBERG, I., RASENAT, S., JUAREZ, M. D. *et al.* 1991 Thermally induced hydrodynamic fluctuations below the onset of electroconvection. *Phys. Rev. Lett.* **67**, 596–599.
- RUCKLIDGE, A. M. 1992 Chaos in models of double convection. *J. Fluid Mech.* **237**, 209–229.
- SHIL'NIKOV, L. P. 1965 A case of the existence of a denumerable number of periodic motions. *Sov. Math. Dokl.* **6**, 163–166.
- SPARROW, C. 1982 *The Lorenz Equations: Bifurcations, Chaos and Strange Attractors*. Springer.

- TAVENER, S. J., MULLIN, T. & BLAKE, G. 2001 Numerical bifurcation study of electrohydrodynamic convection in nematic liquid crystals. *Phys. Rev. E* (to appear).
- TSUCHIYA, Y., HORIE, S. & ITAKURA, H. 1988 Coherent pattern oscillation of Williams domain in nematic liquid crystal. *J. Phys. Soc. Japan* **57**, 669–670.
- TURAEV, D. V. & SHIL'NIKOV, L. P. 1987 On bifurcations of a homoclinic 'figure eight' for a saddle with a negative saddle value. *Sov. Math. Dokl.* **34**, 397–401.
- WIGGINS, S. 1988 *Global Bifurcations and Chaos: Analytical Methods*. Springer.
- YANG, C. Y., ITAKURA, H., HORIE, S., TSUCHIYA, Y. & KAWAKUBO, T. 1986 Angle deflective oscillation of the stripe pattern in nematic liquid crystals. *J. Phys. Soc. Japan* **55**, 703–706.